Laser velocimeter turbulence measurements in shrouded and unshrouded radial flow pump impellers

R. D. Flack*, C. P. Hamkinst and D. R. Brady*

Shrouded and unshrouded versions of a four-vaned radial flow impeller with a design flow coefficient of 0.063 were tested in a volute pump using a two-component frequency-shifted laser velocimeter. Velocity and turbulence profiles were measured at six flow rates and at four radial and six circumferential positions in the volute. The variations of the velocity and Reynolds stresses from blade to blade were measured and presented. In general the turbulence intensities ranged from 0.06 to 0.28. Highest levels were measured for the unshrouded impeller. Also, the highest levels were for low flow rates. For higher flow rates the turbulence tended to become more isotropic. The full set of velocity and turbulence data is presented and is intended to be benchmark data against which predictions can be compared.

Keywords: *shrouded pump impellers, unshrouded pump impellers, turbulence measurements, radial flow*

Introduction

Unshrouded pump impellers are very sensitive to the tip clearance: when the clearance is increased, the head and efficiency decrease, and the absorbed power usually falls[1]. The dissipation of the tip leakage in a vortex is a direct energy loss resulting in lower delivered head. At the same time the blades unload and reduce the required torque. Turbulent flows play a significant role in the efficiencies of such pumps.

In order to numerically model these flow problems successfully the conditions to be modelled must be identified and quantitatively understood. This understanding will aid in the development and verification of the numerical techniques. The tools available to the experimentalist have progressed from Pitot tubes to the totally noninvasive Laser Velocimeters (LV). By combining techniques the present day experimentalist can successfully quantify the different factors influencing flow in turbomachines. The objective of the present research was to isolate one of these factors for pump flows: turbulence. The present data will provide an effective benchmark for future analyses of turbulent impeller flows.

A number of studies on the performance of centrifugal pump impellers and experimental methods have been reviewed, for example, in Refs 2 and 3. All of these references are applicable to the present research. However, for the sake of brevity, only the references covering velocity measurements in impellers will be discussed.

Some of the earliest work in the area of turbomachines was performed by Fisher and Thoma[4]. Using a dye injection method in an open impeller, they showed that at low flowrates a nonuniform velocity distribution in alternating passages was present. Following up on their work were measurements by Binder and Knapp[5], who used Pitot probes to determine the mean velocity in the volute region of two high head, high efficiency centrifugal pumps.

Beveridge and Morelli[6] examined the flow of a 2-D impeller with total head pressure probes rotating with the impeller. At design conditions the flow was well behaved, while at higher flow rates separation was noted on the pressure face of the vanes at the inlet.

Lewinsky-Kesslitz[7] used a static pressure and cylindrical yaw probes to measure the average pressure profiles in a pump impeller. At off-design conditions he found the largest circumferential variations.

Fowler[8] measured the velocities in a radial impeller of a centrifugal compressor using a hot wire anemometer. The test rig rotated at 60 r/min but despite the low speed, features of the jet/wake structure were detected.

Lennemann and Howard[9] examined the separation characteristics in shrouded and unshrouded impellers using hydrogen bubble flow visualization. In the shrouded impeller the flow on the blade suction side separated and backflow occurred, while, in the unshrouded impeller, separation was found on the blade pressure side. McDonald, Lenneman and Howard[10] used a hot film probe in a radial shrouded impeller with backswept circular arc blades and found that the formation of the jet/wake was characterized by a region of low velocity at mid-blade height on the suction surface. Later, Howard and Kittmer[11] measured velocities with cylindrical hot film probes in an impeller with and without shrouds. They found that, although the velocities in the passage directions were similar, the cross-passage velocities were strongly influenced by the tip leakage flows.

Moore[12] experimentally measured the effects of rotation and secondary flows in a simple rotating, shrouded radial exit passage with a hot wire anemometer. The jet/wake structure weakened as the flow rate was reduced. One set of turbulence intensity profiles was reported.

Sakurai[13] investigated the separation in a nonrotating impeller with log spiral blades. Using an arrow type pressure probe, he found that the efficiency increased with the increase in outlet/inlet area ratio within the limitations of separation.

Eckardt[14], using pressure transducers, Pitot probes, and hot wire probes made measurements at the exit of a centrifugal compressor impeller with a tip speed of 300 m/s. At these high rotational speeds a jet/wake structure was still observed.

Measurements in an open radial exit centrifugal impeller were taken by Mizuki[15]. Using a four-holded yaw probe inside the impeller, pressure taps and hot wire anemometer, a jet/wake structure was identified over a wide range of operation.

With the development of laser velocimetry, a means of determining velocity components without disturbing the flow

* Department of Mechanical and Aerospace Engineering, University of Virginia, Charlottesville, VA 22901, USA
† KSB AG, Frankenthal, Federal Republic of Germany
Received March 1986 and accepted for publication July 1986

0142-727X/87/010016-10$3.00

was achieved. Eckardt[16] used a variation of the laser velocimeter, the Laser-2-Focus Velocimeter (L2F) which was developed by Schodl[17]. This method was used to study the internal flow of a radial unshrouded compressor impeller. The results showed a nearly uniform entrance velocity profile change to a well-defined jet/wake structure at impeller exit.

Adler and Levy[18] used an LV to investigate the flow in a shrouded centrifugal impeller. At design conditions the flow in the impeller was stable and attached. They also showed the difference in the flow fields between this closed impeller and an open impeller near the shrouds.

Howard *et al*[19] described their LV processing technique in which they measured the velocities in the blade passages of a vertical axis radial pump impeller. The results were preliminary.

Kannemans[20] measured with an LV the velocity profile over the entire blade passage at different flow rates for a shrouded, transparent radial impeller with backswept blades. Results indicated that the flow is unsteady and at low flow rates viscous effects dominate.

In an attempt to correlate the location of the wake, Johnson and Moore[21] measured velocities using a five-hole probe in a shrouded impeller. Comparisons were made between results for the design flow rate and two other flow rates.

Murakami *et al*[22] used an oil surface flow visualization method and cylindrical yaw probe to map the flows in two impellers (seven and three blades). Results from the two impellers were not similar.

Fister *et al*[23] used an L2F to measure the velocities in a 180° bend simulating the bends in multi-stage radial flow turbomachines using water as the flow medium. Measurements showed that the turbulence intensity increased from the outer to the inner wall.

Krain[24], used an L2F to investigate the effects of a vaned and vaneless diffuser on the flow in an impeller in a centrifugal compressor. Midway through the impeller passages an increase in the boundary layer growth on the suction side blade passage was found.

Kämmer and Rautenberg[25] used pressure probes to study the inlet velocities to a centrifugal compressor impeller. Reverse flow was detected near the suction wall, and strong swirl was induced by the impeller when the impeller was operating in the rotating stall region.

McGuire and Gostelow[26] used a small Pitot probe with an enclosed transducer and wall taps to map the flow at the exit of a pump impeller. They evaluated the slip factor.

Hayami *et al*[27] used an L2F to measure velocity profiles in the inducer of a centrifugal compressor. At the design flow rate good agreement was found between measured profiles and ideally predicted profiles. At low flow rates the inducer stalled.

In summary, considerable research has been performed on the velocity measurements in impellers. Almost all of the efforts have concentrated on average velocity or pressure profiles, however. Very little work has been presented on turbulence conditions in impellers. Yet, turbulence is largely responsible for inefficiencies in modern pumps.

To evaluate the turbulent conditions a clear Plexiglas pump with two different clear impellers was tested at different flow rates. A two-directional laser velocimeter was used to map the flow field in the impeller and volute regions. The differences between shrouded and unshrouded impellers in terms of velocity and turbulence profiles are addressed, and results are presented.

Experimental equipment and procedures

Pump and flow loop

The centrifugal pump used in this study was a radial flow machine of constant flow width (12.7mm). The geometry is shown in Figs 1, 2 and 3. The impeller (Fig 1) has four blades with constant blade angles of 16° and discharges into a 7.0° log spiral volute of the same width. The pump is constructed of Plexiglas, and laser velocimeter measurements are possible in the windows shown in Fig 2. The walls of the casing are Plexiglas 50.8 mm thick except in the window regions, where the thickness is reduced to 9.5 mm to allow better transmission of the laser beams.

The volute of the pump is a separately adjustable insert. It can be adjusted off centre to study an impeller operating eccentrically in the volute. For this study the volute was 'centred' on the impeller so that the volute area was linearly increasing with circumferential position. The tip of the cutwater is at an angle $\theta = 7°$.

The flow loop is conventional and consists of a 76.2 mm diameter pipe connected to a tank open to the atmosphere. The flow rate was measured with an orifice plate downstream of the discharge. The total developed head was measured with static pressure taps located in the suction pipe 5 diameters upstream of the impeller and in the discharge of the volute just beyond window 11 in Fig 2. The outputs of the taps were recorded with vertical water manometers. There are flow straighteners 19 pipe diameters before the pump suction side and 9 diameters before the orifice plate. The pump flow rate was set with a globe valve downstream of the orifice plate.

The 25.4 mm drive shaft is supported by two ball bearings. Axial positioning and tip clearances (c_1, see Fig 3) were set with an adjustable sleeve against the pump end (inboard) bearing inner race. The shaft was driven with a belt drive to an induction motor. The belt pulley was placed near the outboard bearing to eliminate transmitted deflections to the impeller. The shaft torque was not measured. The pump running speed is 620 r/min,

Notation

b	Passage width
c_1	Tip clearance
C	Velocity in stationary frame
D	Impeller diameter
H	Total head produced by pump
m	Mean standard deviation
N	Rotational speed
N_b	Number of signals in each 'bin'
N_s	Specific speed $\equiv NQ^{1/2}/H^{3/4}$
Q	Net flow rate through impeller
r	Radius
u	General velocity
u'	General fluctuation velocity
U	Impeller peripheral speed
w	Velocity in rotating frame
θ	Angular position (Fig 2)
ρ	Fluid density
ϕ	Flow coefficient $\equiv Q/2\pi r_2 b_2 U_2$
ψ	Dimensionless head $\equiv gH/U_2^2$

Subscripts

A, B	Orthogonal measurement directions
r	Radial direction
θ	Tangential direction
2	Impeller exit

Superscripts

$\bar{}$	Sample averaged

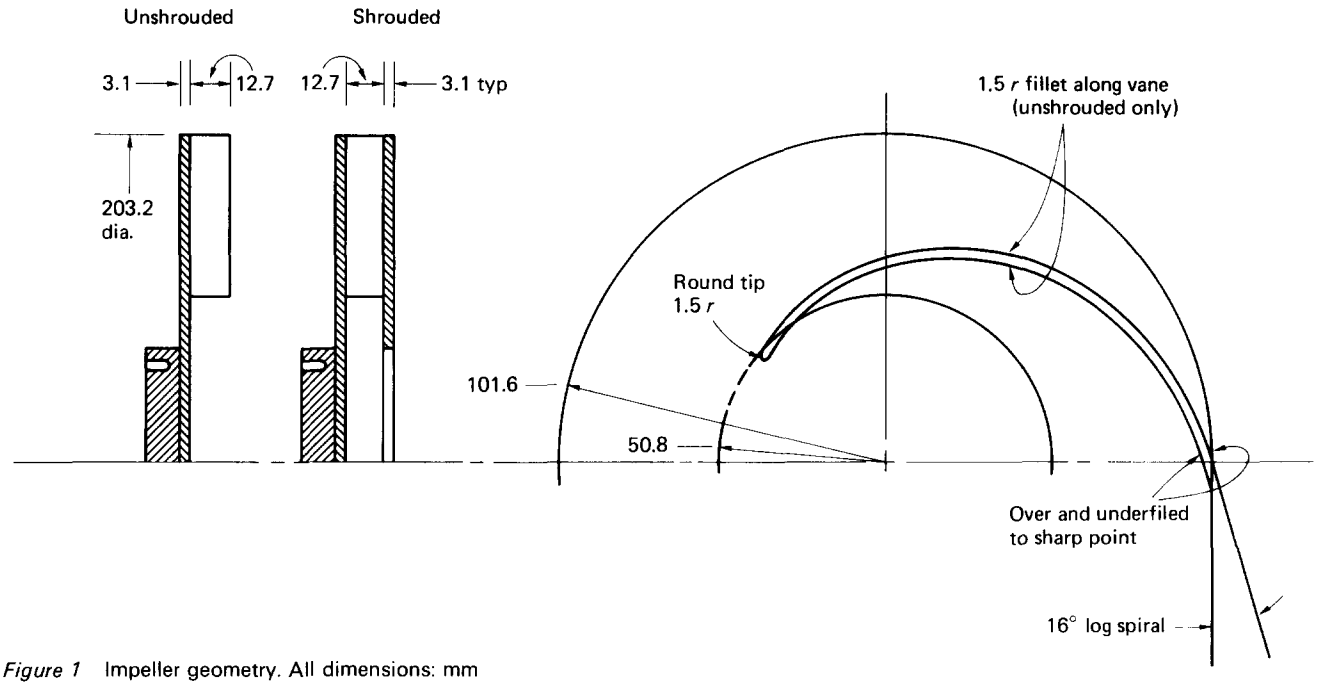

Figure 1 Impeller geometry. All dimensions: mm

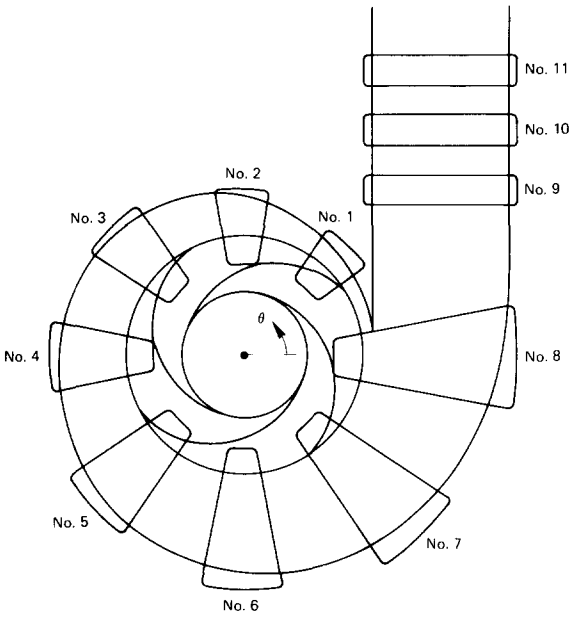

Figure 2 Impeller/volute assembly

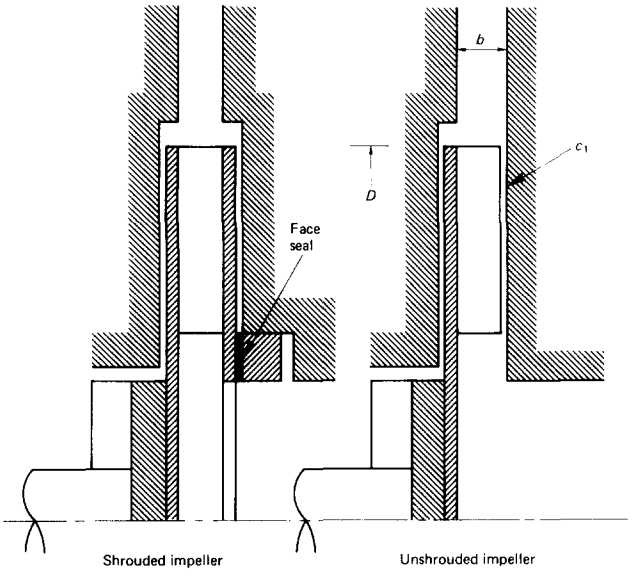

Figure 3 Impeller/casing assembly

and the nominal design flow rate is 31.5 litre/s ($\phi = 0.063$, $N_s = 1200$ US units).

Fig 4 shows the total head flow characteristics of the two impellers. Two tip clearances were tested for the unshrouded impeller ($c_1/b = 0.06$ and 0.08). The velocity head was computed using the average velocities at the pressure tap cross-sections. For both clearances the unshrouded impeller produced significantly lower head than the shrouded version. For all of the following LV results a dimensionless tip clearance (c_1/b) of 0.06 was used. Further details of the pump can be found in Hamkins[28], Flack and Lanes[29] and Thomas *et al*[3].

Laser velocimeter and shaft encoder

The two-dimensional laser velocimeter is a three-beam frequency-shifted system operated in a forward scatter mode. The basic system is shown in Fig 5. The entire optical system is mounted on a mill bed, so that positioning the probe volume in all three directions is possible.

In each beam pair the two beams have different frequencies as a result of frequency shifting. An apparent motion of the fringes results and allows a measurement of the velocity direction as well as magnitude. Measuring velocities in regions of flow reversals is also possible. The frequency shifting is accomplished with a 2-D acoustic optic modulator (Bragg cell), which performs the dual functions of beam separation and frequency shifting. A single beam enters the Bragg cell, and the output of the Bragg cell is a series of diffracted beams (Fig 6). The primary beam (I) is not shifted. The secondary beams (II, III, IV, V) are diffracted and frequency shifted by +15 MHz, +22.5 MHz, −15 MHz, and −22.5 MHz, respectively. A series of higher-order diffractions are also produced. However, only three beams are used (II, III, IV) and the others are optically blocked. Beams II and III form one pair for measuring direction A, while beams III and IV form the pair for measuring direction B, which is perpendicular to direction A. By rotating the Bragg cell through any angle the two sets of perpendicular fringes are also rotated through the same angle. Since the two sets of beams have different shift (or carrier) frequencies, the signal from a single

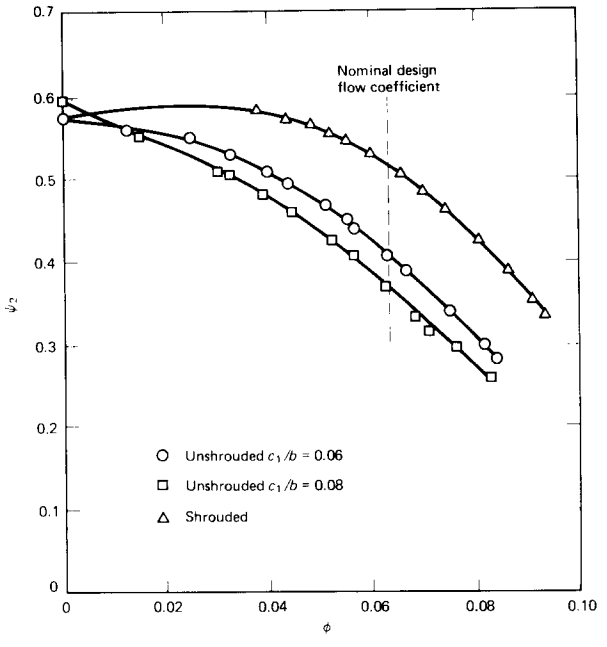

Figure 4 Head-flow characteristics

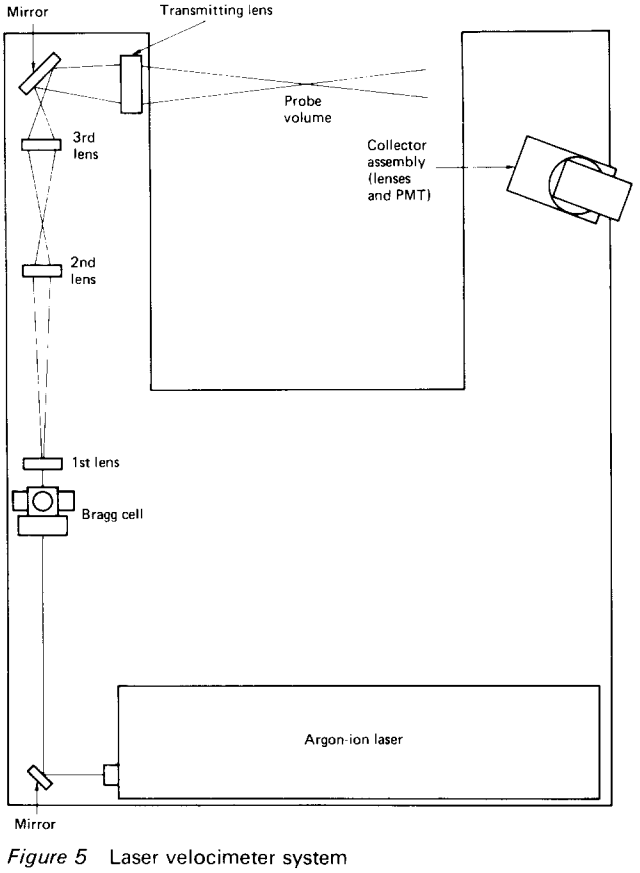

Figure 5 Laser velocimeter system

photomultiplier tube can be separated electronically with filters to simultaneously indicate the two perpendicular velocity components.

The signal processing was accomplished with two burst-type processors having adjustable thresholds levels and five/eight count comparisons with adjustable tolerances. Coincidence checking of the signals from each beam pair was done, and only signals occurring simultaneously on both channels were considered valid.

The outputs of the two processors were two analog voltages calibrated to velocities which were temporarily stored with sample and hold circuits. The impeller angular position was converted into voltage with a shaft encoder; the voltage varied linearly from 0 to 10 V as shaft angular position varied from 0 to 2π. When valid signals occurred simultaneously on both channels, three voltages were recorded: velocity for channel A, velocity for channel B, and the shaft angular position. Each set of data was stored with a dedicated microcomputer onto floppy disks for further processing. The sample and hold circuits then sampled new outputs from the processors.

To obtain LV signals of good quality, appropriate particle seeding in the flow must be present. Microscopic investigations indicated that tap water, after being filtered, contained particles 3 μm and less in diameter and of suitable scattering properties.

Data reduction

In the data processing stage the following were performed.

(1) The data were sorted into 256 separate groups each representing a particular shaft angular position.
(2) For each group, the average velocity and turbulence intensity were computed and transformed to the standard (r, θ) coordinate system.

After the first two steps were performed the effective blade to blade velocity distribution was known for the impeller since an average velocity is associated with each shaft position from 0 to 2π. To obtain more accurate overall result for the blade to blade velocity profiles, passage averaging, step 3, was performed.

(3) The profiles in the four impeller passages were averaged together (each has 64 groups) to obtain an average passage profile.

To obtain sufficient accuracy with a laser anemometer, a large sample size is required. In this study 5000 data points were collected at each measurement location. The signals occurred at random angular positions of the shaft but were sorted into 256 'shaft angle bins' using the shaft encoder data so that the correct average could be computed for each shaft position. Hence, an average of 20 points were used to compute an average velocity for each shaft position.

After a separate average was computed for each of the 256 shaft angle bins, the velocity distributions of the four impeller channels were averaged together into a single average passage of 64 angle bins, each containing N_b data signals (an average of 80) to produce the profiles presented in this paper. Before averaging, the four profiles were identical to within the uncertainty of the data.

The overall average velocity was calculated for each channel and each bin as the mean of the velocity data:

$$\bar{u} = \frac{1}{N_b} \sum_{i=1}^{N_b} u_i \qquad (1)$$

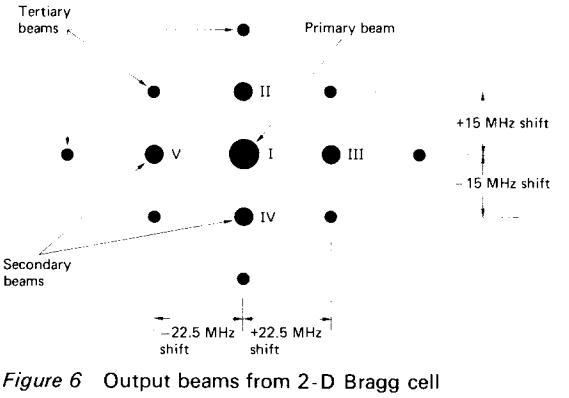

Figure 6 Output beams from 2-D Bragg cell

The mean standard deviation was calculated according to

$$m=\left[\frac{\Sigma u_i^2 - N_b \bar{u}^2}{N_b}\right]^{1/2} \quad (2)$$

The Reynolds stress tensor was obtained from

$$\overline{u'_A u'_A} = m_A^2 \quad (3a)$$

$$\overline{u'_B u'_B} = m_B^2 \quad (3b)$$

and

$$\overline{u'_A u'_B} = \frac{1}{N_b}\left[\sum_{i=1}^{N_b} u_{Ai} u_{Bi}\right] - \bar{u}_A \bar{u}_B \quad (3c)$$

The average velocities and Reynolds stresses were transformed to the (r, θ) coordinate system using the usual rules for vector and tensor transformation.

Uncertainty

The probe volume could be positioned within an accuracy of 0.025 mm radially and 1.0 mm axially. The angular uncertainty of the laser beam orientation with respect to the reference axes 0.6°; this is the limiting factor in computing flow direction. The uncertainty in average velocity components is approximately 2.6% with the sample sizes used. The uncertainty of the Reynolds stresses is 6.0%. ψ is uncertain by 1.5% and the uncertainty in ϕ is 0.0006. These uncertainties do not include the effect of positional uncertainty in the presence of velocity gradients.

The position of the probe volume was uncertain, particularly in the axial direction. Since there were spatial velocity gradients, a misplaced probe volume would measure the incorrect velocity. Based on measurements[28] the position uncertainty and velocity gradients result in an additional uncertainty of 2.8% in the radial component and 0.4% in the tangential component, yielding total uncertainties of 3.8% and 2.6% for the radial and tangential components, respectively.

Alternatively, the velocities are uncertain by 2.6%, and the Reynolds stresses are uncertain by 6.0%, but the position at which to assign them is uncertain, as given above. Finally, the uncertainties in the pump construction itself are $D_2 \pm 0.02\%$, $b \pm 2\%$, impeller runout $\pm 0.2\%$ of D_2, and front clearance $\pm 2\%$ of b.

Considerable concern has been expressed about individual realization biasing over the years. For turbulence intensities below 20% Flack[30] has shown the bias on the velocity data is at worst 4%, while for turbulence intensities of 10% the error is at worst 1%. For 90% of the data reported here the turbulence intensity was less than 20%, indicating that this bias was not a major problem.

Results

Blade to blade velocity and turbulence profiles at the axial centreplane of both impellers were measured in six different windows (1, 4, 5, 6, 7 and 8) for four radii and two flow rates. The angular positions of the measurements for the six windows were $\theta = 45°$, 180°, 225°, 270°, 315°, and 0°, respectively. In addition, blade to blade velocity and turbulence profiles were measured at the axial centre of window 6 for seven flow rates. Only representative data are included here. Velocity data are rendered dimensionless by U_2, the tip velocity, while the Reynolds stresses are rendered dimensionless by ρU_2^2.

Variations with flow rate

Fig 7 indicates how the absolute radial and relative tangential velocity profiles at the axial centreplane change with flow rate in window 6 for both impellers. One should note the variation in

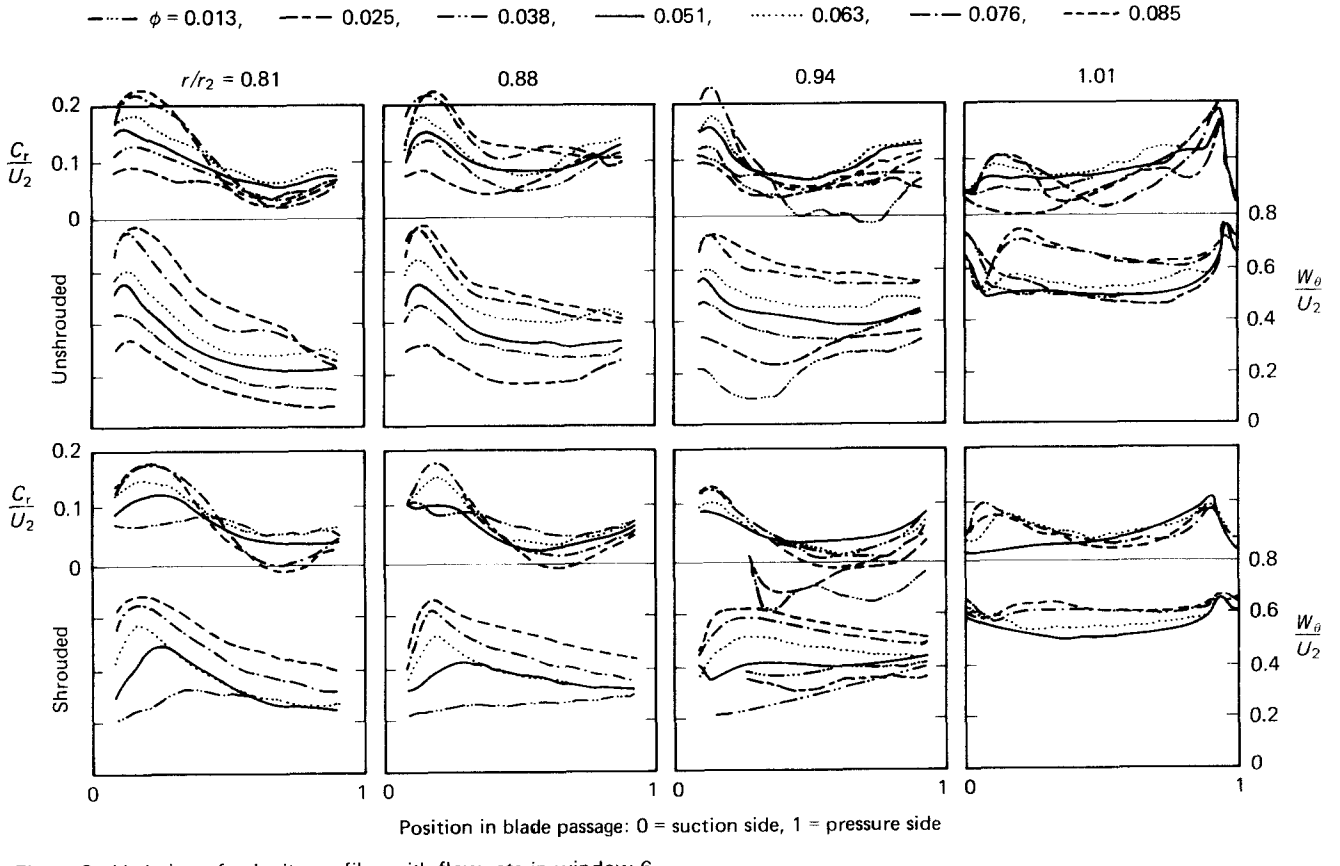

Figure 2 Variation of velocity profiles with flow rate in window 6

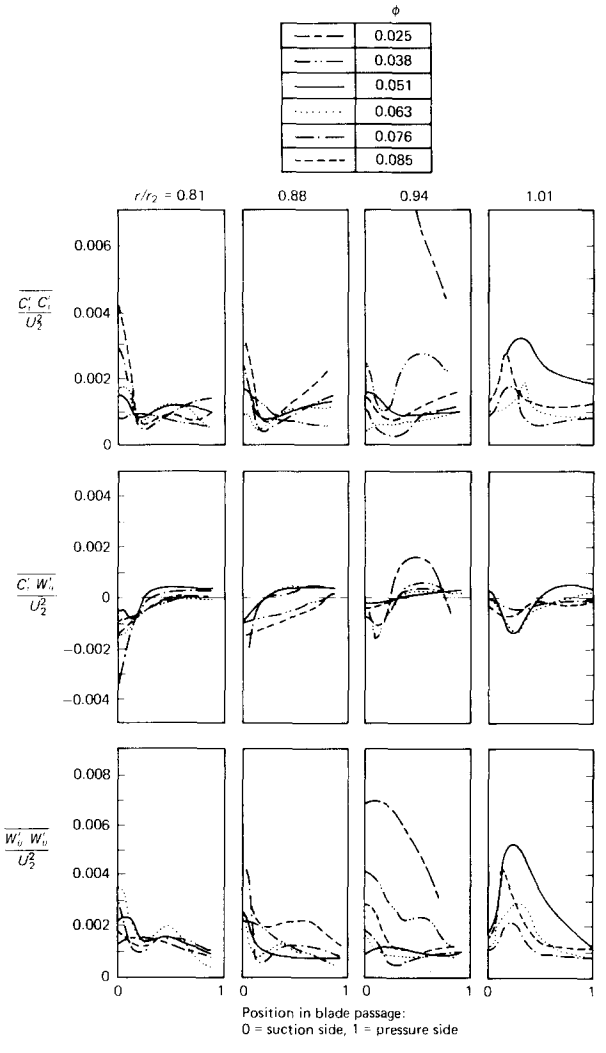

Figure 8 Variation of Reynolds stress profiles with flow rate in window 6—shrouded impeller

velocity gradients from suction to pressure side, which indicates varying blade loadings at the different flow rates. The profiles are most skewed for small radii and become more uniform near the impeller exit. One should also note that in general the blade to blade profiles are more uniform for the shrouded impeller than for the unshrouded impeller.

The measurements here show the same trends as shown by Kannemans[20] and others. Namely, for high flow rates the radial velocity is skewed positively toward the suction side of the passage, particularly for small radii. This trend is also predicted by potential flow theory. For small flow rates the profile is less skewed. In fact Kannemans found for $Q/Q_{\text{Design}} = 0.66$ the profile reversed trends. For the present data the profile became much flatter for small values of ϕ. Just outside of the present impeller ($r/r_2 = 1.01$) the profile reversed trends. Also, the profiles for the unshrouded impeller are seen to be more skewed than for the shrouded impeller.

One should expect better agreement with potential theory at high flow rates than at low flow rates. At low flow rates less momentum is in the boundary layers, and a larger adverse pressure gradient exists due to the increased developed head. These two low flow rate phenomena tend to force thick boundary layers or possibly separated boundary layers, which obviously do not correlate with potential flow. At high flow rates thin boundary layers exist, thus better agreement is found between potential theory and experiment.

Reynolds stress data are presented in Figs 8 and 9. It is worthy of note that the data presented in Figs 8 and 9 are truly turbulence data. They are an average of many data samples at particular locations between blades at particular stationary coordinates and a result of 'random' variations. They are not the same as would be measured with a probe rotating with the impeller, because the probe would sense periodic circumferential variations as well as the 'random' turbulence. The data are the same as if instantaneous data were to be recorded for a series of rotating probes at a particular angular position. In general the largest Reynolds stresses are observed for the lowest flow rates ($\phi \lesssim 0.038$). Also, the absolute value of the cross component of the Reynolds stress is largest for small flow rates, indicating the flow is not isotropic for these cases. At higher flow rates the cross component tends towards zero and the flow becomes more isotropic, particularly for small radii. Maximum turbulence intensities for this window range from 0.20 to 0.06 for the shrouded impeller and 0.28 to 0.10 for the unshrouded impeller as ϕ increases from 0.013 to 0.085. Also, the blade to blade profile change shape significantly as the flow rate is increased, particularly for large radii. The profiles changed more for the unshrouded impeller than for the shrouded impeller.

Variations with circumferential position

Velocities were measured in six windows as indicated above. In the previous section window 6 was covered in detail. For benchmark usage, representative variations of the profiles are presented for all of the windows. These data are for $\phi = 0.051$

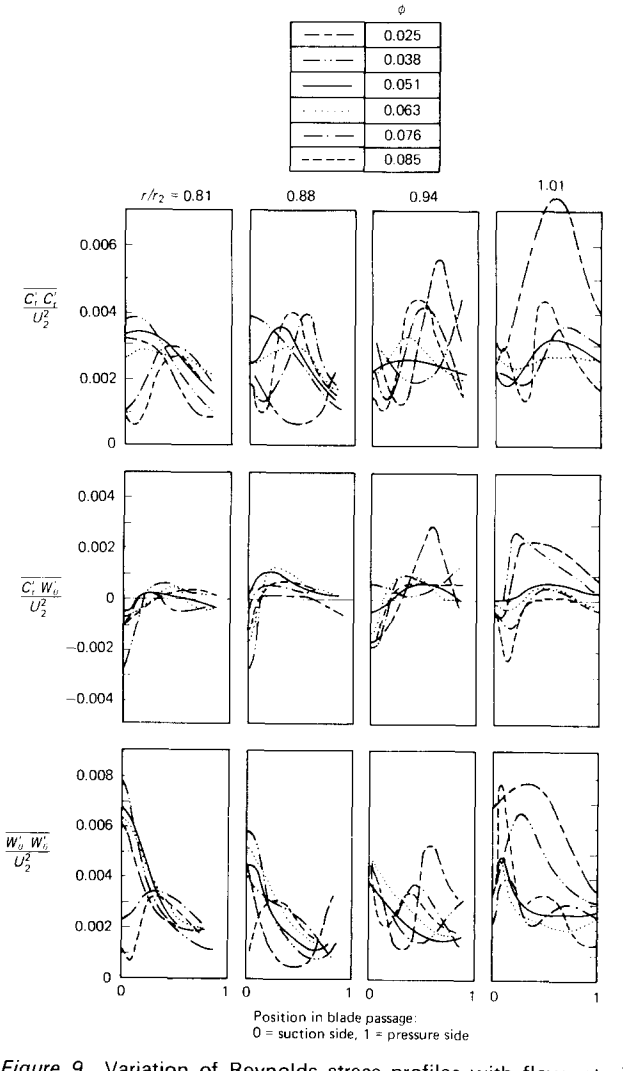

Figure 9 Variation of Reynolds stress profiles with flow rate in window 6—unshrouded impeller

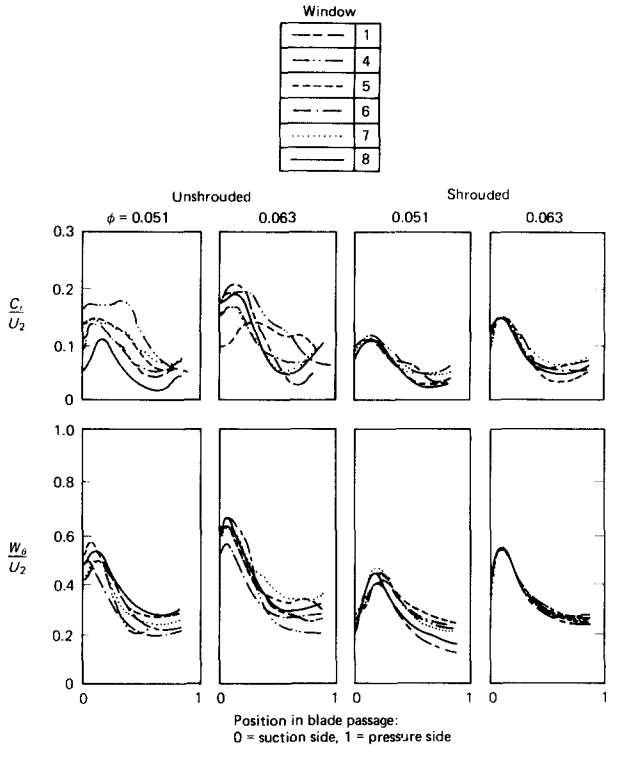

Figure 10 Variation of velocity profiles with circumferential position for both impellers and two flow rates—$r/r_2 = 0.81$

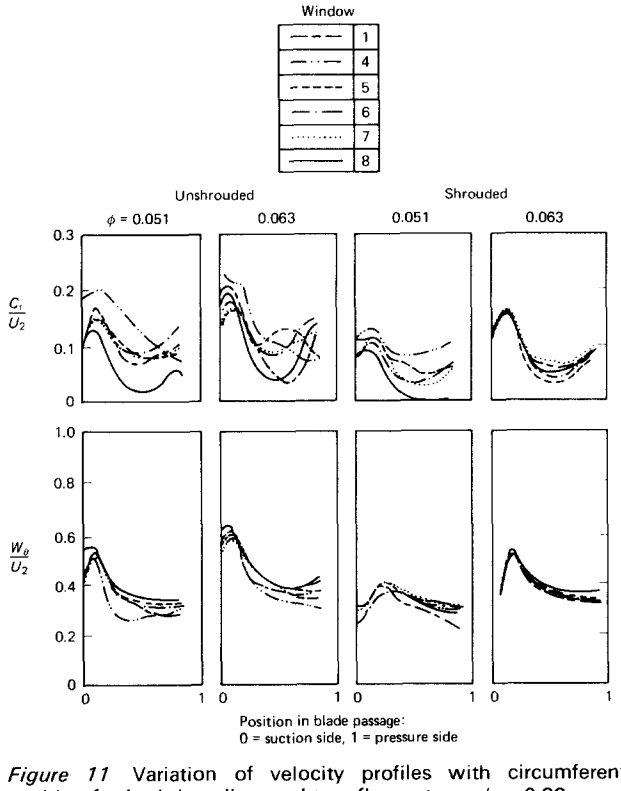

Figure 11 Variation of velocity profiles with circumferential position for both impellers and two flow rates—$r/r_2 = 0.88$

and $\phi = 0.063$, four radii, and both impellers (Figs 10–13). Reynolds stress data for the same conditions are presented in Figs 14–17.

In some cases velocity profiles which exhibit kinematic similitude at all windows are observed: for example, shrouded impeller at $r/r_2 = 0.81$. In other cases, however, much different profiles are observed in the different windows: for example, shrouded impeller at $r/r_2 = 1.01$. At the off-design flow rate ($\phi = 0.051$), circumferential variations of the profiles are more pronounced for both impellers. By comparing the shrouded and unshrouded profiles, one can also observe that the shrouded impeller exhibits more circumferential similitude than does the unshrouded impeller at all radii.

In Figs 14–17 Reynolds stresses are presented for the six

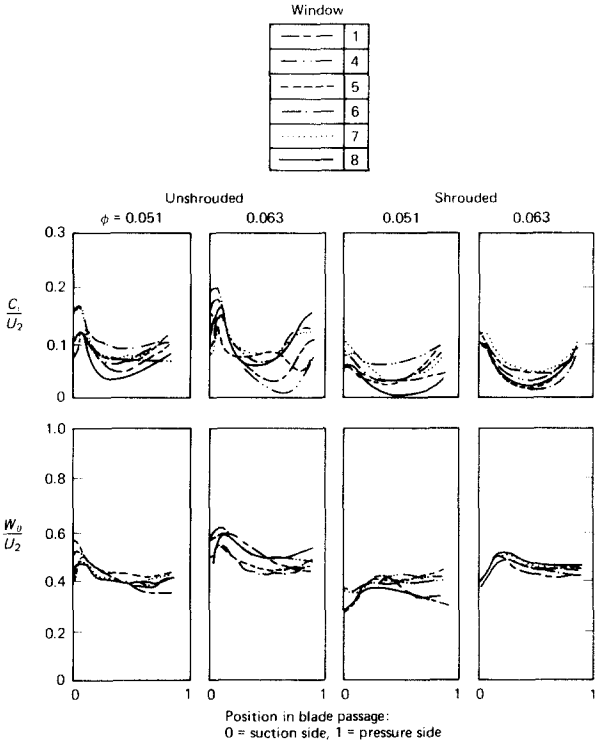

Figure 12 Variation of velocity profiles with circumferential position for both impellers and two flow rates—$r/r_2 = 0.94$

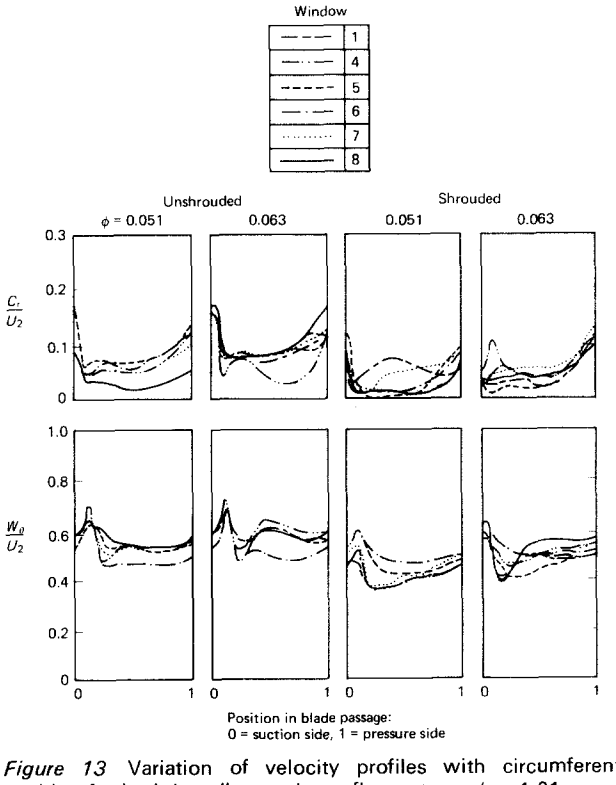

Figure 13 Variation of velocity profiles with circumferential position for both impellers and two flow rates—$r/r_2 = 1.01$

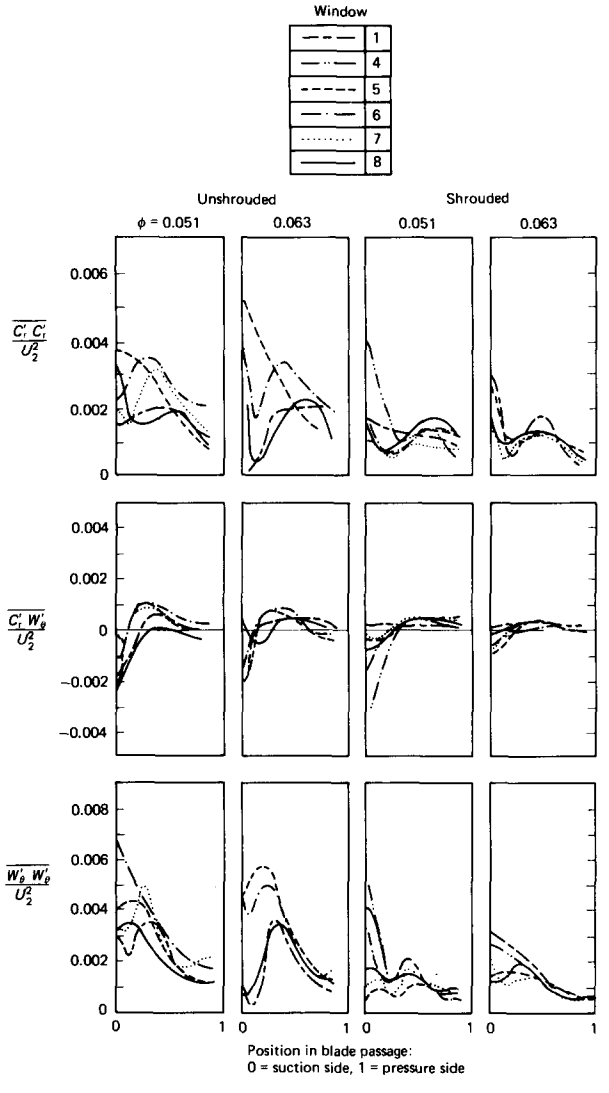

Figure 14 Variation of Reynolds stress profiles with circumferential position for both impellers and two flow rates—$r/r_2 = 0.81$

windows and the same conditions above. Once again, circumferential similitude is observed in some cases and not in others. For example, the blade to blade Reynolds stress profiles are similar for $r/r_2 = 0.88$ and 0.94 for the shrouded impeller at $\phi = 0.063$. However, for off-design flow rates, or for the unshrouded impeller, or for small or large values of r/r_2, the Reynolds stress profiles become more functions of θ.

General trends

By considering Figs 8–9 and Figs 14–17 several general observations can be made on the turbulence. In general, turbulence levels are much higher everywhere in the unshrouded impeller than in the shrouded one. This should really not be surprising given the unbounded nature of the flow as well as tip leakage.

The same basic trends are observed in both the shrouded and unshrouded impellers. The normal components of the Reynolds stress tensor are generally highest on the suction side of the passage, and fall towards the pressure side, although significant departures from this trend are observed for flows above or below the design point. The cross component of the Reynolds stress is in general negative near the suction side of the passage but becomes positive towards the pressure side.

Similar trends are found for the velocity profiles. Namely, the largest velocities are usually found near the suction surface. When the turbulence fluctuations and time-averaged velocities are combined, the blade to blade turbulence intensity profiles are found to be fairly uniform across the channel, indicating that no particular region is more turbulent than another. According to several turbulence models[31,32] the suction side of a passage should be more stable, and the pressure side should have increased turbulence. This is not observed in this study, however.

The turbulence is also very high in the exit region of the impeller. The region just outside the impeller is an area of intense mixing of jet flow with the blade wakes and is therefore subject to large turbulence.

Summary and conclusions

Velocities and Reynolds stresses in shrouded and unshrouded versions of an impeller in a radial flow volute pump with a design flow coefficient of 0.063 were studied. The quantities were measured at various radial and circumferential positions and for various flow rates with a two-directional laser velocimeter. Velocity and Reynolds stress profiles in the blade to blade and hub to shroud planes were obtained. The data can be used for benchmarking ongoing prediction methods. The important conclusins are as follows.

(1) Blade to blade velocity profiles were more uniform in the shrouded impeller than the unshrouded impeller.

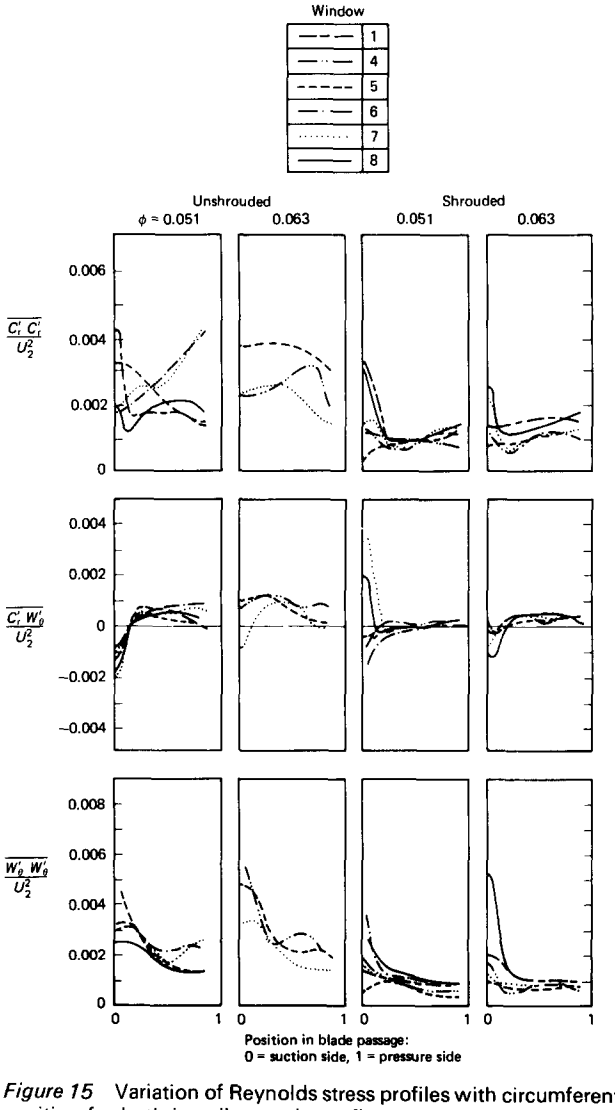

Figure 15 Variation of Reynolds stress profiles with circumferential position for both impellers and two flow rates—$r/r_2 = 0.88$

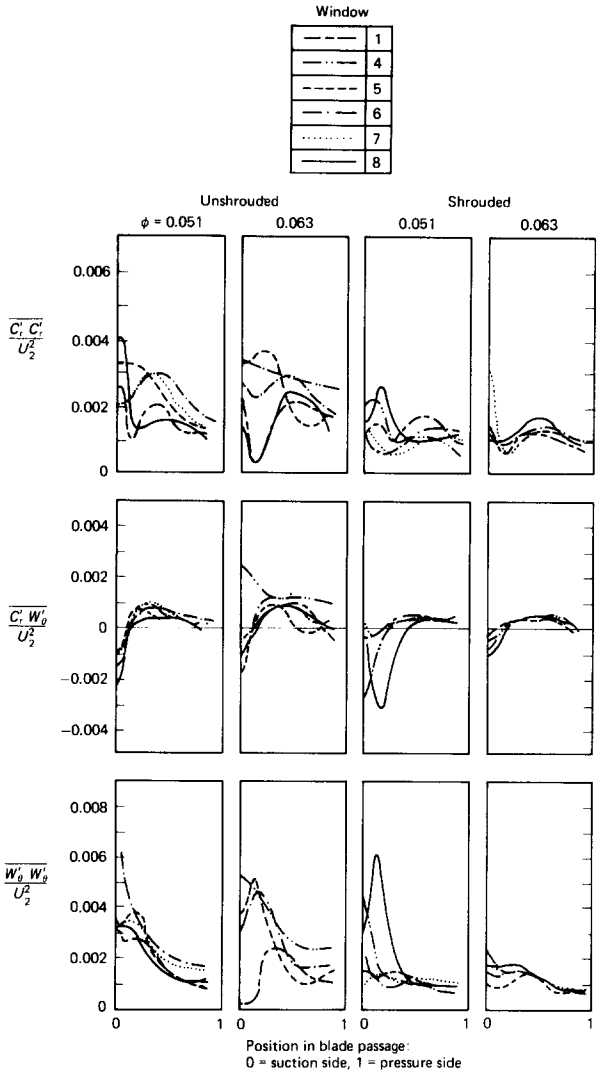

Figure 16 Variation of Reynolds stress profiles with circumferential position for both impellers and two flow rates—$r/r_2 = 0.94$

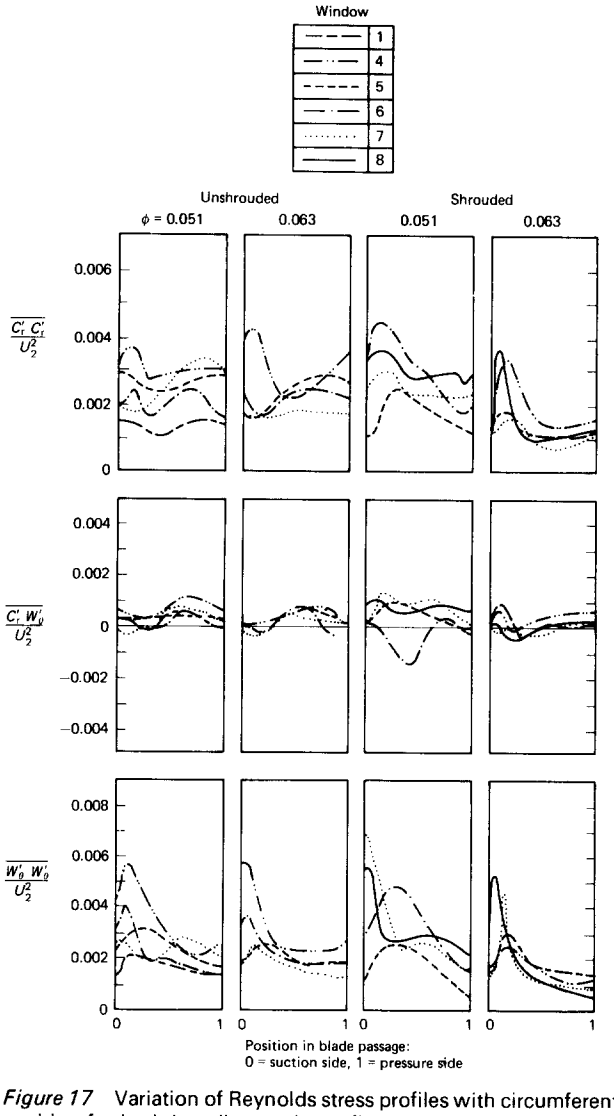

Figure 17 Variation of Reynolds stress profiles with circumferential position for both impellers and two flow rates—$r/r_2 = 1.01$

(2) The velocity profiles were also more uniform near the exit of the impellers than for smaller radii.
(3) Velocity profiles exhibited more circumferential similitude for small radii and/or on-design flow rates than for large radii and/or off-design flow rates.
(4) Maximum turbulence intensities ranged from 0.06 to 0.20 for the shrouded impeller and 0.10 to 0.28 for the unshrouded impeller as ϕ decreased.
(5) The largest Reynolds stresses were observed for low flow rates ($\phi \lesssim 0.038$). Also, the turbulence tended to become more isotropic for higher flow rates ($\phi \gtrsim 0.038$).
(6) The highest turbulence levels were measured for large radii.
(7) Near the design point the normal components of the Reynolds stress were highest on the suction side of the passage. The cross component of Reynolds stress was negative near the suction side but increased toward the pressure side.

Acknowledgements

This work was sponsored in part by the NASA-Lewis Research Center under Contract No. NAG3-180, in part by the ROMAC Industrial Research Program at the University of Virginia, and in part by Goulds Pumps, Inc.

References

1 Japikse, D. *Introduction to Turbomachinery Analysis*, Concepts ETI, Hanover, NH, August 1981
2 Brownell, R. B. and Flack, R. D. Flow characteristics in the volute and tongue region of a centrifugal pump. *Paper No.* 84-GT-82, ASME International Gas Turbine Conference, The Netherlands, 1984
3 Thomas, R. N., Kostrzewsky, G. J. and Flack, R. D. Laser velocimeter measurements in a pump volute with a non-rotating impeller. *Int. J. Heat and Fluid Flow*, in press
4 Fisher, K. and Thoma, D. Investigations of the flow conditions in a centrifugal pump. *Trans. ASME*, HYD-54-8, 1932
5 Binder, R. C. and Knapp, R. T. Experimental determinations of the flow characteristics in the volutes of centrifugal pumps, *Trans. ASME* 1936, **58**, 649–661
6 Beveridge, J. H. and Morelli, D. A. Evaluation of a two-dimensional centrifugal pump impeller. *ASME Paper No.* 50-A-147, 1950
7 Lewinsky, Kesslitz, H. P. Ein Verfahren zur Ermittlung des Stromungsverlaufes in einer Radialpumpe. *Osterreichische Ingenieur-Z.* 1959, **3**(10), 330–336
8 Fowler, H. S. The distribution and stability of flow in a rotating channel. *J. Eng. for Power, Trans. ASME* 1968, **90**(3), 229–236
9 Lennemann, E. and Howard, L. H. G. Unsteady flow phenomena in rotating centrifugal impeller passages. *J. Eng. for Power, Trans. ASME* 1970, **92**(1), 65–72
10 McDonald, G. B., Lennemann, E. and Howard, J. H. G. Measured and predicted flow near the exit of a radial flow impeller. *J. Eng. for Power, Trans. ASME* 1971, **93**(4), 441–446

11 Howard, J. H. G. and Kittmer, C. W. Measured passage velocities in a radial impeller with shrouded and unshrouded configurations. *J. Eng. for Power, Trans. ASME* 1975, **97**(2), 207–213

12 Moore, J. A wake and eddy in a rotating radial flow passage. *J. Eng. for Power, Trans. ASME* 1973, **95**(3), 205–219

13 Sakurai, T. Flow separation and performance of decelerating channels for centrifugal turbomachines. *J. Eng. for Power, Trans. ASME* July 1975, **97**(3), 388–394

14 Eckardt, D. Detailed flow investigations within a high speed centrifugal impeller. *J. Fluids Eng., Trans. ASME* Sept. 1976, **98**(3), 390–402

15 Mizuki, S., Hattore, T., Arign, I. and Watanabe, I. Reverse flow phenomena within centrifugal compressor channels at lower flow rates. *ASME Paper* No. 76-GT-86, 1976

16 Eckardt, D. Instantaneous measurements in the jet/wake discharge flow of a centrifugal compressor impeller. *J. Eng. for Power, Trans. ASME*, July 1975, **97**(3), 337–346

17 Schodl, R. A Laser-Two Focus (L2F) Velocimeter for automatic flow vector measurements in the rotating components of turbomachines. *J. Fluids Eng., Trans. ASME*, December 1980, **102**(4), 412–419

18 Adler, D. and Levy, Y. A laser–Doppler investigation of the flow inside a backswept, closed, centrifugal impeller. *J. Mech. Eng. Sci.* 1979, **21**(1), 1–6

19 Howard, J. H. G., Mukker, O. S. and Naeem, T. Laser Doppler measurements in a radial pump impeller. In *Measurement Methods in Rotating Components of Turbomachinery*, ASME Publication I00130, 1980, 113–138

20 Kannemans, H. Radial pump impeller measurements using a laser Doppler velocimeter. *ASME Paper* No. 80-GT-94, 1980

21 Johnson, M. W. and Moore, J. The development of wake flow in a centrifugal impeller. *J. Eng. for Power, Trans. ASME*, April 1980, **102**(2), 382–390

22 Murakami, M., Kikuyama, K. and Asakura, E. Velocity and pressure distributions in the impeller passages of centrifugal pumps. *J. Fluids Eng., Trans. ASME*, December 1980, **102**(4), 420–426

23 Fister, W., Zahn, G. and Tasche, J. Theoretical and experimental investigations about vaneless return channels of multi-stage radial flow turbomachines. *ASME Paper* No. 82-GT-209, 1982

24 Krain, H. A study on centrifugal impeller and diffuser flow. *J. Eng. for Power, Trans. ASME*, October 1981, **103**(4), 688–697

25 Kämmer, N. and Rautenberg, M. An experimental investigation of rotating stall flow in a centrifugal compressor. *ASME Paper* No. 82-GT-82, 1982

26 McGuire, J. T. and Gostelow, J. P. Experimental determination of centrifugal impeller discharge flow and slip factor. *ASME Paper* No. 85-GT-77, 1985

27 Hayami, H., Senoo, Y. and Ueki, H. Flow in the inducer of a centrifugal compressor measured with a laser velocimeter. *J. Eng. for Gas Turbines and Power, Trans. ASME*, April 1985, **107**(2), 534–540

28 Hamkins, C. P. Laser velocimeter measurements in a shrouded and unshrouded radial flow pump impeller. *MS Thesis*, University of Virginia, Department of Mechanical and Aerospace Engineering, May 1985

29 Flack, R. D. and Lanes, R. F. Effects of volute geometry and impeller orbit on the hydraulic performance of a centrifugal pump. In *Performance Characteristics of Hydraulic Turbines and Pumps, ASME Publication* H00280, 1983, 127–133

30 Flack, R. D. Influence of turbulence scale and structure on individual realization laser velocimeter biases. *J. Phys. E — Sci. Instrum.*, October 1982, **15**(10), 1038–1044

31 Howard, J. H. G., Patankar, S. V. and Bordynuik, R. M. Flow prediction in rotating ducts using Coriolis-modified turbulence models. *J. Fluids Eng., Trans. ASME*, December 1980, **102**(4), 456–461

32 Koyama, H., Masuda, S., Ariga, I. and Watanabe, I. Stabilizing and destabilizing effects of Coriolis force on two dimensional laminar and turbulent boundary layers. *J. Eng. for Power, Trans. ASME*, January 1979, **101**(1), 23–31